Additive Manufacturing 33 (2020) 101130

Contents lists available at ScienceDirect

Additive Manufacturing

journal homepage: www.elsevier.com/locate/addma

A review of additive manufacturing of cermets

Atefeh Aramian[a,b], Seyed Mohammad Javad Razavi[b], Zohreh Sadeghian[a], Filippo Berto[b,*]

[a] Department of Material Science and Engineering, Faculty of Engineering, Shahid Chamran University of Ahvaz, Golestan Boulevard, 6135785311, Ahvaz, Iran
[b] Department of Mechanical and Industrial Engineering, Norwegian University of Science and Technology NTNU, Richard Birkelans vei 2b, 7491 Trondheim, Norway

ARTICLE INFO

Keywords:
Additive manufacturing
Cermet
Hard metal
Selective laser sintering/melting
Binder jet additive 3D printing

ABSTRACT

Cermets are a category of materials including ceramic and metallic phases, which possess the combined properties of both phases. Over the last few decades, numerous conventional processes such as powder metallurgy techinques and casting have been proposed for the fabrication of cermet components. In recent years, additive manufacturing (AM) has emerged as a promising method that can eliminate most of the limitations of conventional production methods. Among AM processes, selective laser sintering/melting (SLS/SLM), laser engineering net shaping (LENS), direct laser fabrication (DLF), binder jet 3D printing, and 3D gel/direct-ink-write/robocasting printing have been investigated for manufacturing bulk cermet parts. This study presents a summary of research that has been conducted to produce bulk cermets by additive manufacturing.

1. Introduction

Cermets, as engineered composites, have high hardness and toughness which are respectively typical properties of ceramics (reinforcement phase) and metals (binder phase). Ceramic phases include carbides, nitrides, oxides, and carbonitrides of titanium, molybdenum, tungsten, tantalum, niobium, and vanadium, while nickel, cobalt, molybdenum alloys, etc., are usually used as the metallic binder [1,2]. Cermets have been used for cutting and forming applications, abrasive slurry nozzles, mechanical seal rings, bearings, and coatings for erosion and corrosion protection due to their favorable properties which include mechanical properties, excellent wear and oxidation resistance, and thermal stability. They have also received increasing attention for ballistic impact protection [3–9]. The first generation of cermets (WC-Co) emerged in 1927 and subsequently different types of ceramics and metals have been used to produce and improve the properties of cermets. Currently, WC-Co, TiC, and Ti(C,N)-based cermets with binders such as Fe, Co, Ni, Mo, and the alloys thereof have been used in various industrial applications [6,10].

Fabrication methods such as conventional powder metallurgy techniques (PM), hot pressing (HP), hot isostatic pressing (HIP), self-propagating high temperature synthesis (SHS), spark plasma sintering (SPS), mechanical alloying (MA), carbothermal and thermite reduction, and casting methods have been used to produce cermets in the past. Moreover, a few surface modification methods such as plasma spraying, reactive flame spraying, tungsten-inert gas (TIG) arc melting, and laser surface treatment have been applied to the fabrication of cermet cladding materials and coatings [5,11–23].

Manufacturing of cermets by conventional methods involves restrictions such as limitations in geometrical complexity and size, requirement of excessive equipment for methods such as die casting, time and cost intensive post-processing, and difficult machining processes. The AM technique, which has the potential to reduce production cost by reduction of material loss and number of fabrication steps, has been investigated recently as an alternative fabrication method for the production of bulk cermets [24,25].

2. Additive manufacturing of cermets

Over the last decade, AM has been considered as an attractive technique for *layer-by-layer* fabrication of complex *and intricately-shaped* components. AM process is classified into three categories based on the feedstock; namely, powder-based, liquid-based, and solid-based techniques [26]. Thus far, selective laser sintering/melting (SLS/SLM), binder jet (3D printing), laser engineering net shaping (LENS), and direct laser deposition (DLD), as powder-based processes, have been used for cermet fabrication. In addition, 3D gel/direct-ink-write/robocasting printing AM technology, a combination of gel-casting and material extrusion, has recently been applied to cermet production [27,28]. Fig. 1 shows cermet samples that have been produced by different AM processes.

There is limited literature related to the fabrication of cermets by AM techniques, most of which are concerned with the production of conventional hard metal (WC with different binder). This research

* Corresponding author.
E-mail address: filippo.berto@ntnu.no (F. Berto).

https://doi.org/10.1016/j.addma.2020.101130
Received 24 July 2019; Received in revised form 12 February 2020; Accepted 13 February 2020
Available online 13 February 2020

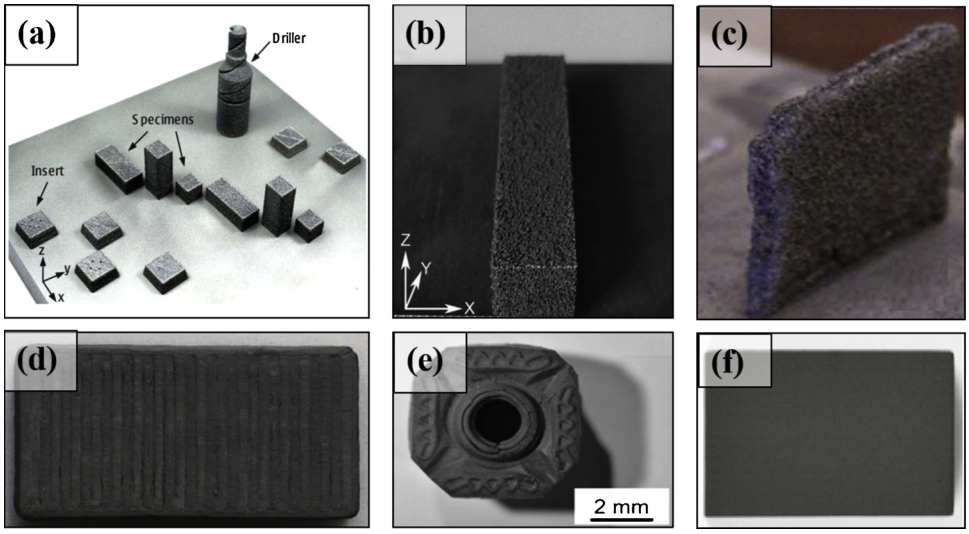

Fig. 1. Cermet samples produced by a) selective laser melting [29], b) direct laser sintering [30], c) laser engineering net shaping [31], d) binder jet [32], and e) Extrusion-Based 3D-Printing [33], f) 3D gel printing [34].

mostly focuses on the process parameters required to produce dense and crack-free components, and include investigations of limited properties such as density, hardness, and wear behavior. For brevity, a summary of the researches related to the fabrication of cermets is presented in Table 1.

It is worth mentioning that there are few numbers of literature in terms of printing cermet coatings by SLM [35], SLS [36,37] and LENS process [38,39] which are not considered in this paper.

2.1. Selective laser melting (SLM)

SLM is one of the AM techniques based on powder metallurgy and laser technology. In this technique, components are produced by the selective fusion of a powder layer based on a 3D CAD model of the required component in the protective gas environment like argon gas [41]. This process includes heating and fusing of the powdered material from which the component is to be printed by a high energy laser beam, followed by rapid solidification of the molten pool (see Fig. 2) [76,77].

One of the important factors in the SLM process is the powder properties (in addition to composition and purity, morphology, size, and size distribution uniformity) which affect the microstructural and mechanical properties of SLM products [78,79]. Chen et al. [46] reported that the sample manufactured by granular powder had higher density with less porosity and defects in comparison with irregular shape powder. Generally, gas atomized powders are used for SLM due to their excellent flowability, but different milling processes have been used for the preparation of powder mixtures to be used for the SLM process in a few studies [40,42]. In addition, some researchers have used processes such as cladding, magnetron sputtering, cold spray chemical vapor deposition (CVD), etc. to form a thin metal layer on the ceramic powder in order to attain uniform distribution of metallic binder on ceramic powder and surface modification of ceramic powder [41,80–82]. During the SLM process, each parameter has a specific effect on the properties of the resultant product. For instance, decreasing the scanning speed leads to melting pool expansion and a higher density of the final product, while increasing the laser power or reducing the scan line spacing result in lower porosity. A schematic illustration of SLM process parameters is shown in Fig. 3. According to the literature, large temperature gradients can lead to the formation of cracks and residual stresses in SLM products [42] which are the most challenging aspects of AM of cermets. Although a few techniques such as in-situ temperature control have been proposed to decrease the thermal gradient during the SLM process, in the presence of the easily fusible phase (metal), partial powder sintering during the leveling cycle is more likely to occur, interrupting the manufacturing process [29,42]. In association with 3D-printing of WC-Co cermets, high volumetric energy density leads to a high relative density of components, which causes pronounced embrittlement of the processed WC-Co. Moreover, at both high and low energy density, the tendency of crack formation is high regardless of the values of the other process parameters. In porous components, single cracks are mostly formed between the pores, while in non-porous parts, cracks grow continuously to considerably longer lengths than those of porous ones.

Khmyrov et al. [44] investigated the phase formation during the manufacturing of WC- x wt.% Co (x: 75, 72.4, 50, 6). The results revealed a complete dissolution of WC in all SLM specimens except for the sample containing 6 wt.% Co. They reported the dissolution of WC, formation of β-Co(W,C) solid solution in all samples and small amount of W_4Co_2C (in samples containing 75 and 72.4 wt.% Co) or W_3Co_3C (in samples containing 50 wt.% Co). Though W_2C was formed in the sample with 6 wt.% Co content, some WC remained in the structure. Scholars attributed the dissolution of WC and the formation of different carbides to the reduction of carbon content in the manufactured samples.

As an effort to produce crack-free WC-Co samples, Khmyrov et al. [43] used two powder compositions of 75 wt.% and 50 wt.% Co content. In order to reach a uniform distribution in the powder, the powder mixture was milled for 2 h at 200 rpm rotating speed. SLM samples were fabricated using a hatching distance of 100 μm and 50 W power with a scanning speed of 100 mm/s. The sample containing 75 % Co was crack free; while the formation of cracks in the sample with 50 % Co could not be avoided (see Fig. 4). The presence of cracks in the sample with 50 % Co content was attributed to the formation of the brittle W_3Co_3C phase during the SLM process. Moreover, a direct relationship between the hardness of metal-ceramic composites and the size of the carbide particles after the production process was reported [28,43].

Grigoriev et al. [45] and Campanelli et al. [47] also reported the formation of cracks in the manufactured specimens which had high hard phase (WC) content. It was explained by the considerable difference between the melting point of WC and binder material as well as the thermal expansion coefficient mismatch.

Domashenkov et al. [42] investigated the microstructure and mechanical properties of WC-12 % Co samples produced by SLM using two sets of powders namely; conventional powder (manufactured sample named standard sample) and nanophase powder. The conventional

Table 1
Research on additively manufactured cermets.

Process	Authors & year	Composition	Process parameter					Description
			Laser power	Scan speed	Hatch distance	Layer thickness	Type of laser	
SLM	GU et al. (2010) [40]	In situ formation of WC/Ni_2W_4C From W-Ni- C powder	2.55 KW/mm^2	0.8 m /s 1.0 m/ s 1.2 m/ s	0.15mm	0.1 mm	CO_2	–
	Davydova et al. (2014) [41]	B_4C-Co	60 W	100mm/s 150mm/s 200mm/s 250mm/s 300 mm/s	70 μm	50 μm	–	–
	Uhlmann et al. (2015) [29]	WC-17%Co	**Energy density**				–	–
			1667 J/mm^3		185 J/mm^3			
	Domashenkov et al. (2016) [42]	WC-12%Co (coarse and fine)	**Single layer**					–
			40 W	130 mm/s	–	40 μm	–	
			3D printing					
	Khmyrov et al. (2017) [43]	25%WC- Co	40 W	130 mm/s	90 μm	40 μm	–	–
			Single layer					
		50%WC- Co	80 W	10–50 mm/s	–	100 μm	–	
			3D printing					
			30 to 50 W	100 mm/s	50 μm	35 μm	–	
	Khmyrov et al. (2017) [44]	WC- 75 wt.% Co BK8- 70 wt.% Co WC- 50 wt.% Co WC- 6 wt.% Co	50 W	100 mm/s	–	40 μm	–	–
	Grigoriev et al. (2019) [45]	WC- 6 wt.% Co	30–70 W	30-350 mm/s	70 μm	10–100 μm	–	–
	Chen et al. (2019) [46]	WC- 20 wt.% Co	380–400 W	470–500 mm/s	60–75 μm	50 μm	–	–
	Campanelli et al. (2019) [47]	WC- 10 wt.% Co - 4 wt.% Cr	100 W	40–100 mm/s	120 μm	30 μm	Nd:YAG	–

(*continued on next page*)

Table 1 (*continued*)

Process	Authors & year	Composition	Process parameter					Description
			Laser power	**Scan speed**	**Hatch distance**	**Layer thickness**	**Type of laser**	
SLS	Wang et al. (2002) [48]	WC- 9% Co	8.18 W 17.9 W 28.1 W	10 mm/s 25 mm/s	–	0.1–0.5 mm	Nd:YAG	Manufactured parts were porous
	Gu et al. (2006) [49]	(WC-10 %Co) / 80Cu	700 W	0.06 m/s	0.15 mm	–	–	Spot size 0.30 mm
	Gu and Shen (2006) [50]	WC-10% Co/Cu 20:80, 30:70, 40:60	700 W	0.06 m/s	0.15 mm.	0.3 mm	CO_2	–
	Ga°ard et al. (2006) [51]	(Fe,Ni)–30, 60, 80 wt.% TiC					CO_2	–
	Gu et al. (2007) [52]	(WC-Co:Cu,50:50) (WC-Co:Cu:La2O3 50:49:1)	700 W	0.06 m/s	0.15 mm.	0.20 mm	CO_2	–
	Gu and Shen (2008) [30]	WC-10% Co/Cu nanocomposites	700 W	0.05 mm/s	0.15 mm	0.20 mm	CO_2	Spot size 0.30 mm
	Kumar et al. (2008) [53]	WC-18Cu-12Co WC-9% Co WC-50% Co	**(WC-18Cu-12Co & WC/ 12%Co) Samples** 40 W	–	0.1 mm	0.3 mm	CO_2	Post processing: bronze infiltration
			(WC/ 9%Co) Sample 50–25W	–	0.1 mm	0.5–0.3 mm	CO_2	
	Kumar (2009) [54]	WC-18% Cu-12% Co WC-12% Co WC- 9% Co	**(WC-18Cu-12Co & WC/ 12%Co) Samples** 40W	–	0.1 mm	0.3 mm	CO_2	Post processing: bronze infiltration
			(WC/ 9%Co) Sample 50–25W	–	0.1 mm	0.5–0.3 mm	CO_2	
	Sun et al. (2009) [55]	Zr–ZrB2, (30, 35, 40, 50 wt.% Zr)	65–152 W	0.6–4 mm/s	–	100 and 500 μm	wave diode laser	–
	Kyogoku et al. (2012) [56]	WC-10% Co WC-10% Co/30% Cu WC-10% Co/Cu-20% Sn	10～50W	5～30 mm/s	0.1～0.3 mm	–	Ytterbium fiber	–
	Filippov et al. (2016) [57]	Ti-B_4C	**SLS** 1 KW	0.5 m/min	–	–	CO_2	–
			SLM 0.5 KW	0.5, 0.7, & 1 m/min	–	–	CO_2	
	Kumar et al. (2017) [58]	WC-17% Co	270 W	500 mm/s	0.04 mm	0.04 mm	–	Powder bed temperature: 200°C
	Cavaleiro et al. (2017) [59]	WC- 13 wt% stainless steel AISI 304L	39 - 72 W	75–10mm/s	0.08 mm	100 μm	Ytterbium fiber	–
	Kumar (2018) [60]	WC-17% Co	270 W	500 mm/s	0.04 mm	0.04 mm	–	Powder bed temperature: 200°C
Laser engineering net shaping (LENS)	Xiong et al. (2008) [61]	WC-10% Co	**Power**	**Traverse speed**	**Powder feed rate**	**Working plane**	Nd:YAG	Inhomogeneous microstructure with coarse particles
			140-200 W	2–11 mm/s	7–21 g/min	Focal plane ± 4 mm		
	Xiong et al. (2009) [62]	WC-10% Co	200 W	3 mm/s	10 g/min	–	Nd:YAG	–
	Xiong et al. (2010) [63]	(Ti,W)C-Ni	260–300 W	2–4 mm/s	3–5 g/min	0.13 mm per layer	Nd:YAG	–
Direct Laser Fabrication	Li et al. (2009) [64]	TiC-(Ni:20, 30, 40 Vol%)	**Power**	**Traverse speed**	**Powder feed rate**	**Laser beam size**	CO_2	–
			2400–2600 W	200 mm/min	1.5–1.8 g/min	3.5×3.5 mm		

(*continued on next page*)

Table 1 (*continued*)

Process	Authors & year	Composition	Process parameter					Description
			Laser power	Scan speed	Hatch distance	Layer thickness	Type of laser	
Binder jet 3D printing	Kernan (2007) [65]	WC-10% Co	**Nozzle diameter**	**Layer thickness**	**Printing speed**		–	Post processing: sintering
			127 μm		**2.0 m/s**			
	Paul D. and Collins (2018) [66]	WC- Co	–	–	–		–	–
	Enneti et al. (2019) [32]	WC-12% Co	–	–	–		–	Post processing: sintering
	Enneti and Prough (2019) [67]	WC-12% Co	–	50 – 70 μm.	100 mm/s		–	Post processing: sintering
	Maderud and De Flon (2019) [68]	WC- Co	–	–	–		–	–
Extrusion-Based 3D-Printig	Lengauer et al. (2019) [33]	**Fused-Filament Fabrication (FFF)** / **Composite Extrusion Modelling (CEM)**		–			–	–
		WC-10Co)&(Ti(C,N)Co/ Ni-based)-organic binder / WC-Co polymer granulate						
	Michael et al. (2018) [69]	WC-10Co)&(Ti(C,N)Co/ Ni-based)-organic binder / WC-Co polymer granulate		–			–	–
3D gel-printing	Zhang et al. (2018) [34]	WC-20%Co	**Nozzle diameter**	**Layer thickness**	**Printing speed**		–	Post-processing: sintering
			0.50 mm	0.35 mm	0.28 mm/s			
			0.60 mm	0.45 mm				
			0.70 mm	0.55 mm				
Thermoplastic 3D Printing (T3DP)	Scheithauer et al. (2017) [70]	WC-10%Co	150 μm	–	–		–	Post-processing: HIP

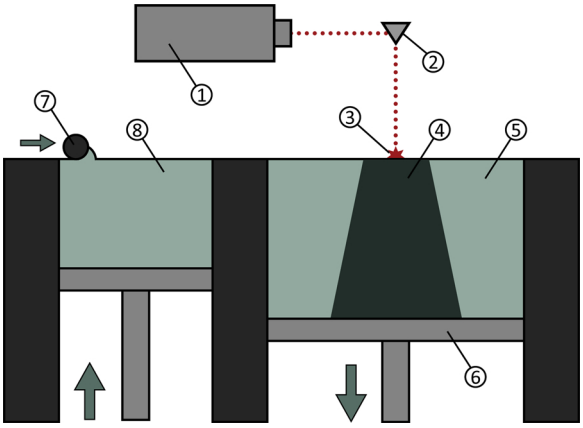

Fig. 2. Schematic illustration of SLS/SLM process: (1) laser, (2) scanner system, (3) molten pool, (4) printed object, (5) powder bed, (6) build platform, (7) powder roller, and (8) new powder stock.

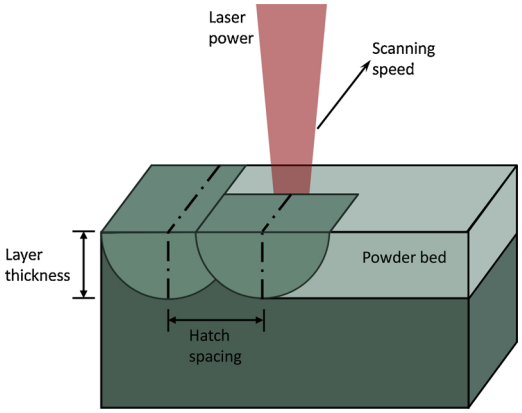

Fig. 3. Schematic illustration of exposure parameters affecting volumetric energy density (EV) in the SLM process.

composite was produced by the agglomeration and sintering of WC and Co powders. They reported the formation of W_2C and W_2Co_4C as a result of WC decarburization during the melting and solidification process. According to the experimental observations, two regions containing coarse and fine carbides were observed in the samples (Fig. 5). Hardness values were reported to depend on the size of carbides in both samples produced by conventional and nanophase powders. Higher hardness values were obtained in regions containing finer carbides as shown in the Table 2. Moreover, due to repetitive thermal cycling during the SLM process, the crystal size in both samples increased. In the sample prepared from the nanostructured powder, the crystallite size of WC increased from 10 ± 3 nm to 180 ± 50 nm, and in the conventional sample it increased from 56 ± 6 nm to 330 ± 100 nm [42].

It is worth mentioning that the fraction of the matrix and the mean free path of dislocations within the matrix strongly affect the resulting hardness, and decreasing these factors increases the hardness [83]. Gu et. al [40]. reported successful in-situ fabrication of $WC/Ni_2W_4C(M_6C)$ from W-Ni-graphite powder mixture by SLM process with the following parameters: laser power; 2.55 kW/ mm^2, scan speeds; 1.2 m /s, 1.0 m /s, and 0.8 m /s, hatch spacing 0.15 mm, and layer thickness: 0.1 mm. The procedure resulted in the high hardness of the final material due to the physical nature of as-prepared WC-based hard metals and induced residual stresses during the SLM process.

Hardness measurements revealed the maximum microhardness value of 1870.9 $HV_{0.1}$ in WC phase compared to those of binder and WC/binder interface (Fig. 6). This hardness value was reported to be higher than that of WC-Co hardmetals produced by laser engineering net shaping (1437 $HV_{0.1}$ [42]), nanocrystalline WC-Co produced by spark plasma sintering (700–1500 $HV_{0.1}$ [84]), and laser clad WC/Ni layer on H13 tool steel substrate (650 $HV_{0.1}$ [85]).

It was reported that decreasing the scan speed, the quantity and shape of the porosities changes from a large number of small and elongated porosities to a few spherical porosities. Therefore, the relative density increased with reducing scan speed (see Fig. 7) [40].

Davydova et al. [41] used the CVD process to fabricate B_4C/(Co-based metal) by pure boron and Co_3B phase. Their research resulted in porous specimens (37 % porosity which mainly placed at interlayer area) with some micro cracks. The microstructure of the samples revealed that due to insufficient volume of the metal layer, the molten metal layer could not fill the voids between particles, which led to the formation of porosity in the sample. In terms of mechanical properties, compression testing showed the maximum strength to be about 110 MPa. This low compressive strength was attributed to the low strength at the metal/ceramic interface and the number of overall porosities in the samples. Fig. 8 shows the propagation of the cracks at the interface between the metal matrix and boron carbide after strength measurements. The hardness measurement conducted on metal and ceramic zones showed 600 $HV_{0.3}$ and 2900–3200 $HV_{0.3}$ Vickers hardness, respectively.

2.2. Selective laser sintering (SLS)

Another process that has been used for 3D-printing of cermets is selective laser sintering (SLS). Powder preparation and process parameters of the SLS process are quite similar to those of the SLM process [59,86]. Usually, SLS-produced cermets are post-processed. In a few studies, the manufacturing of cermet samples by SLS was followed by an infiltration process [53,54]. Similar to the SLM process, SLS process parameters play an important role in sample production. For instance, high laser power leads to increased crack nucleation and accordingly porosity, and large hatch distance causes the delamination of sintered components. Hence, it is essential to optimize the process parameters for each material based on the desired properties and the geometry of the part [53,58]. Up to now, scholars tried different process parameters and chemical composition in order to reach the optimum process parameters and appropriate mechanical properties.

Kumar and Czekanski [58] investigated the effect of different SLS process parameters such as power (270 − 370 W) and scan speed (900 − 1100 mm/s) as well as preheating of powder bed on

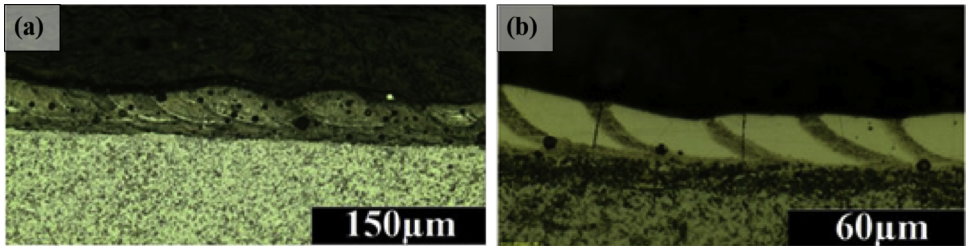

Fig. 4. Cross-section of the remelted powder layer on the substrate, a)75 wt.% Co, and 50 wt.% Co [42].

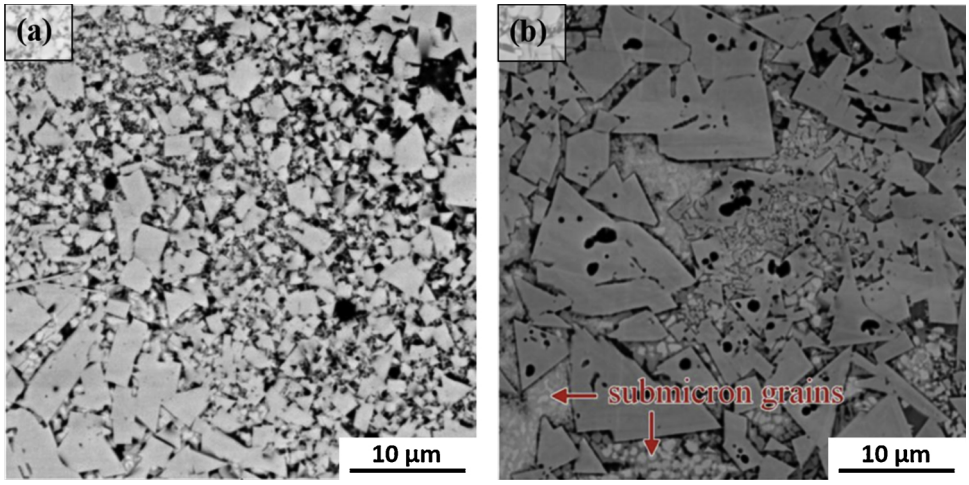

Fig. 5. Microstructure structure of the samples obtained from (a) nano phase, and (b) conventional WC/12Co powders [42].

Table 2
Microhardness results obtained from nano phase and conventional WC/12Co powders [42].

Micro hardness($HV_{0.3}$)	Coarse zone(Nano phase sample)	Fine zone(Nano phase sample)	Coarse zone(Standard sample)	Fine zone(Standard sample)
Average	1496	1542	1384	1515
Minimum	1400	1429	1053	1153
Maximum	1588	1697	1588	1660

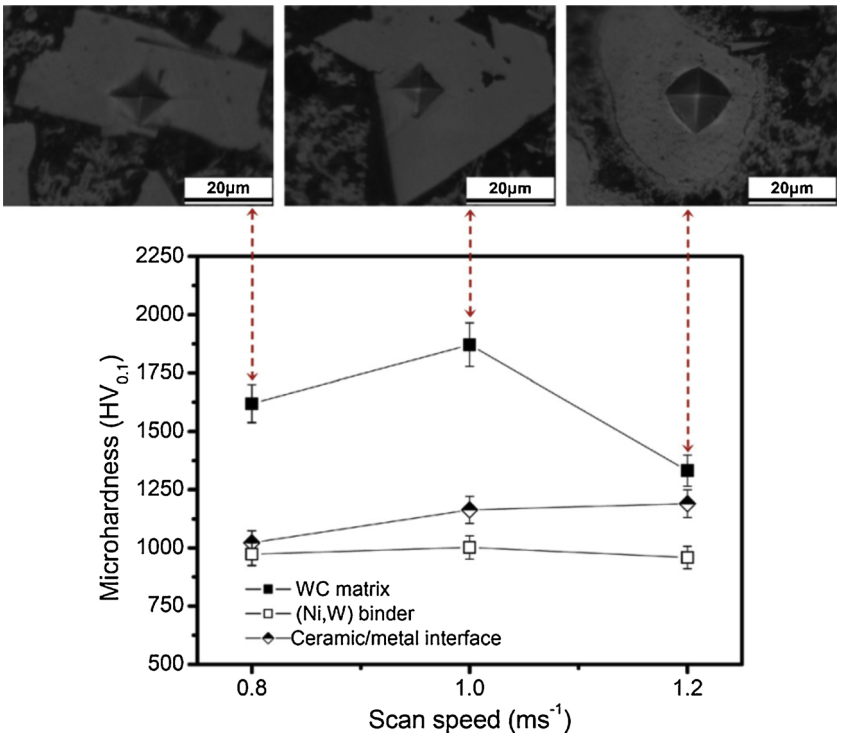

Fig. 6. Effect of scan speed on microhardness of different phases of the SLMed sample (corresponding micrographs at different indents are shown above) [40].

microstructure and hardness of the (WC-17Co) manufactured samples. Microstructural investigation revealed that in both cases (with and without preheating of powder bed) the size and amount of porosities decreased by increasing the input energy density. In addition, by increasing the input energy density, large and connected cracks changed to small and hair-line emerged cracks with preheating the powder bed. Moreover, optical observations did not show any trend of the size and formation of cracks by changing the power or scan speed in manufactured samples without preheating. Fig. 9 shows the cracks and porosities on the samples produced without and with preheating of the powder bed.

Preheating of the powder bed results in more uniform variations of the hardness compared to SLS without preheating. It is believed that the uniform hardness is due to holding the samples at a high temperature for a long time, which is most likely working as an annealing treatment for the samples [58].

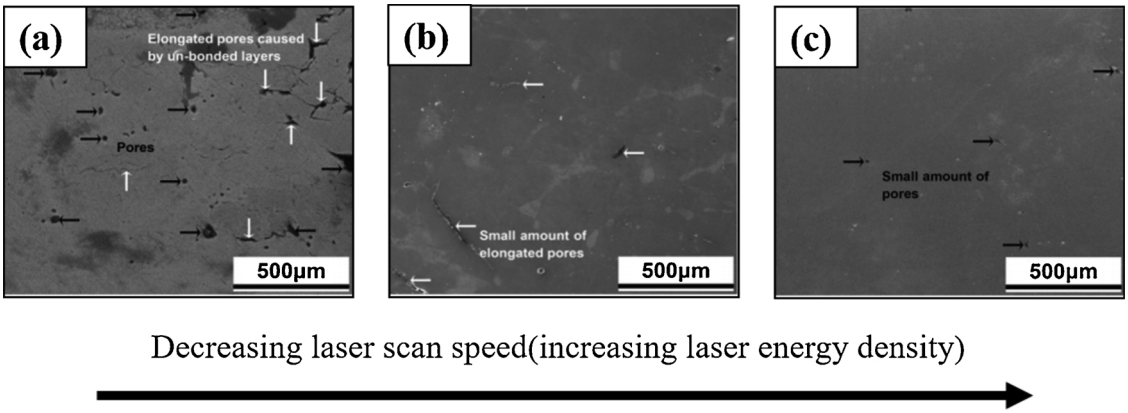

Fig. 7. Low-magnification cross-sectional SEM images of SLM processed samples at (a) 1.2 m/s, (b) 1.0 m/s, (c) 0.8 m/s laser scan speeds [40].

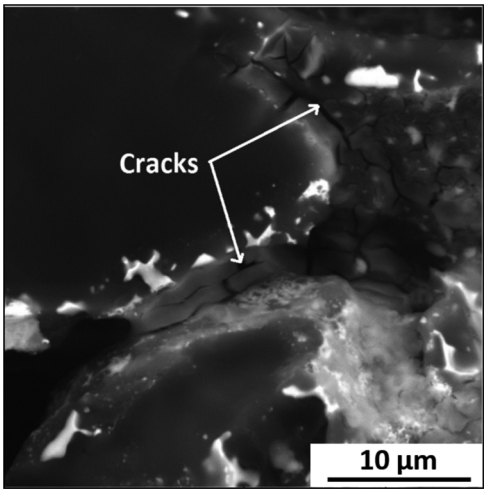

Fig. 8. SEM image of the interface between the metal matrix and boron carbide grains after strength measurements [41].

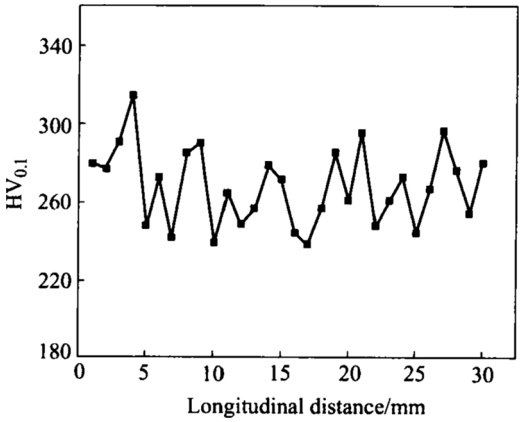

Fig. 10. Variation of the microhardness across the cross-section of the SLS sample [49].

Kumar [60] also investigated the effect of heat treatment (holding at 400, 600, 800 and 1000 °C for three hours) on the hardness and wear behaviour of the manufactured specimens. The results showed that heat treatment can improve the mechanical properties of the components fabricated by SLS. In fact, the heat treatment facilitates the diffusion of the elements leading to the homogenization as well as the formation of the eta phases M_6C and $M_{12}C$.

Gu et al. [49] fabricated WC-10 %Co cermet by SLS and surveyed the microhardness across the cross-section. The results showed hardness fluctuations in the longitudinal section of the sample; as a result of the inhomogeneous distribution of WC particles (Fig.10).

Gu et al. [52] investigated the resulting relative density of SLS samples with the addition of a rare earth oxide (La_2O_3) to WC-Co/Cu powder (50(WC-Co):49Cu:La_2O_3 in weight ratio). An increase in the relative density and microhardness was reported for the sample containing La_2O_3 (Fig. 11). Moreover, the addition of La_2O_3 was reported to enhance the coherency of particles/matrix interface and refine the grain structure of fabricated samples. These improvements were attributed to the effect of La_2O_3 on decreasing the surface tension of the melt and increasing the heterogeneous nucleation rate.

Laser sintering of hardmetals bulk WC-10Co/Cu (60(WC-10Co):40Cu in weight ratio) were successfully fabricated by Gu and Shen [30]. The optimized relative density of 94.3 % and minimal dimensional deformation and balling phenomena were reported by these researchers.

The sintering mechanism during SLS processing of WC-10Co/Cu is shown in Fig. 12, which is the common mechanism in the laser sintering

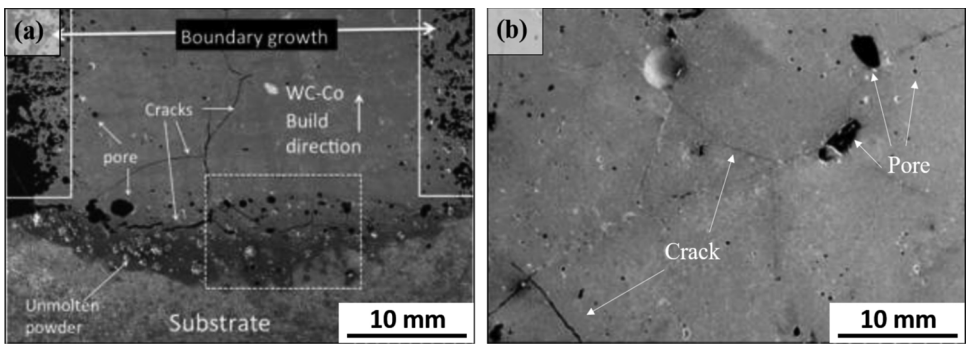

Fig. 9. SEM images of the manufactured sample, (a) without and (b) with preheating of powder bed [58].

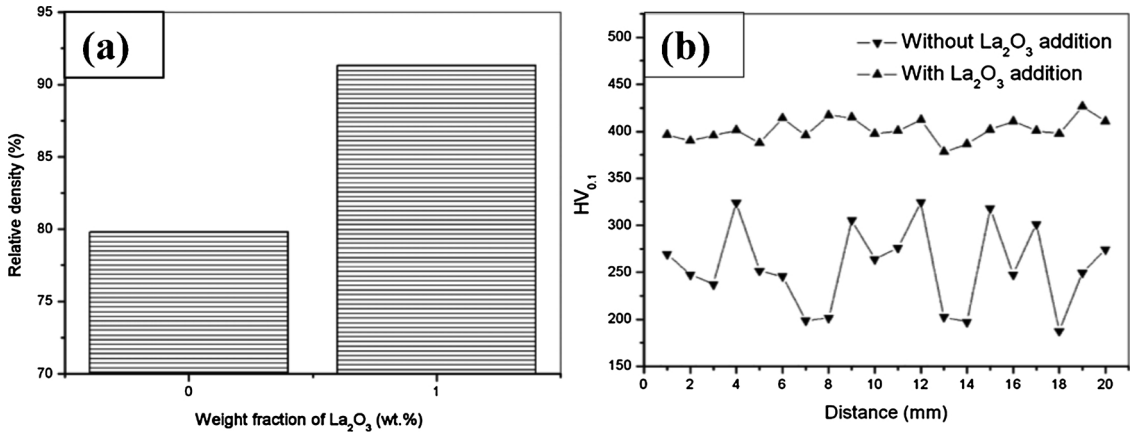

Fig. 11. Effect of La_2O_3 addition on (a) the relative density and (b) microhardness along the vertical section of the manufactured samples [52].

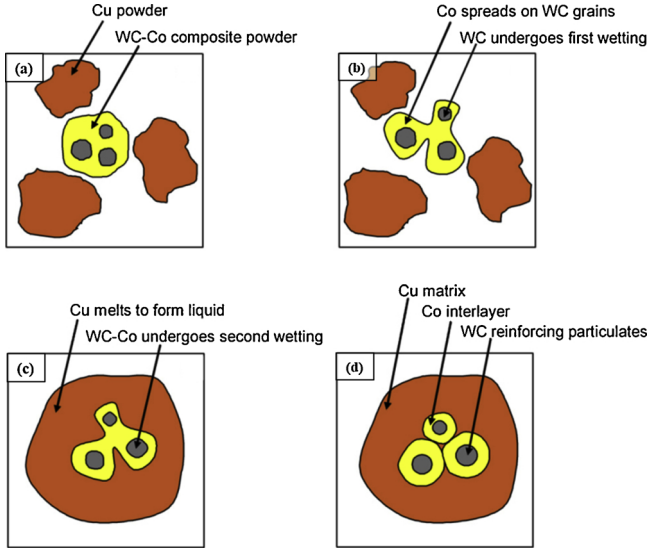

Fig. 12. Schematic illustration of the double stage wetting mechanism during direct laser sintering of the WC-Co/Cu composite system [30].

of conventional hard metals. At the initial stage of wetting, WC particles are homogeneously coated with Co. When the temperature exceeds the melting point of Cu matrix, a larger melted phase so-called “sintering pool” forms. Due to the Gaussian laser beam, a large temperature gradient between the edge and center of the melt pool has emerged that leads to the Marangoni convection. Marangoni convection increases the capability of the liquid flow, which results in the wetting of the WC-Co system by liquid Cu (this is known as the second stage of wetting). Due to the double stage wetting of WC particles, adequate particle reordering and consequently homogenous distribution of WC phase in the metal matrix happens. Moreover, nano-size reinforcing particles were stated to restrict the matrix expansion (by reducing the coefficient of thermal expansion), which is suitable for the formation of coherent and crack free particle/matrix interface.

Dealing with the mechanical properties of SLS cermets, the presence of internal porosities can be significantly detrimental. For this reason, the infiltration of SLS parts has been considered as a post-processing technique to improve both the density of the parts and its mechanical properties. Kumar et al. [53,54] performed wear tests on WC-Co samples with and without bronze infiltration and the results revealed improved mechanical properties of the infiltrated samples. The infiltration resulted in such high wear resistance properties that the SLS parts were reported to be suitable for the production of cutting tools. Additionally, electrical discharge machining (EDM) was suggested as a suitable post-processing technique providing higher wear resistance in SLS cermets compared to diamond polishing. Due to the very high friction coefficient in SLS parts, they are still not an option for molding applications. Further process optimization can be done to obtain SLS cermets with low friction coefficient which are applicable for molding purposes (Fig. 13).

In terms of using the coated ceramic powder for the production of cermets, Cavaleiro et al. [59] used WC powder coated with nanocrystalline stainless steel (SS). The powder was coated by the magnetron sputtering process. It has been stated that using nano crystalline coating leads to improving the powder bed distribution and packing and consequently improves the quality of the sintered part [87].

In addition, the lower melting point of nanocrystalline (SS) due to nano character results in liquid phase sintering at lower temperature and suitable spreading of the binder between WC particles, which improves the density of the sample. Microstructural evolutions of the cermets fabricated by SLS were compared with those manufactured by conventional sintering (vacuum sintering). Large dense WC particles surrounded by Fe-rich binder could be seen in SLS specimens and ring-shaped areas were formed at the interface of WC particles and binder. This phase precipitates during the cooling. In the specimen made by the conventional method η-phase surrounded by WC particles could be seen (Fig. 14) [59].

With regard to the fabrication of tungsten free cermets, Gåård et al. [51] used a direct metal laser sintering process to produced (Fe,Ni)–TiC with different TiC content (30, 60 and 80 wt.%). Their investigation showed that by exceeding the TiC content more than 30 wt.% crack formation in the SLS sample is unavoidable. The crack formation was attributed to the decisive effect of the coefficient of thermal expansion

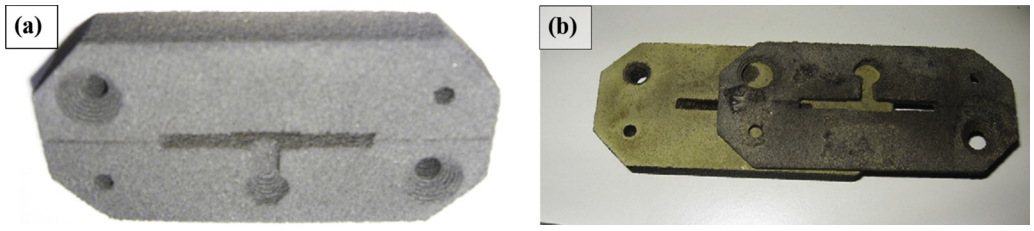

Fig. 13. Injection mold produced from WC-9% Co cermet using the SLS process before and after bronze infiltration [54].

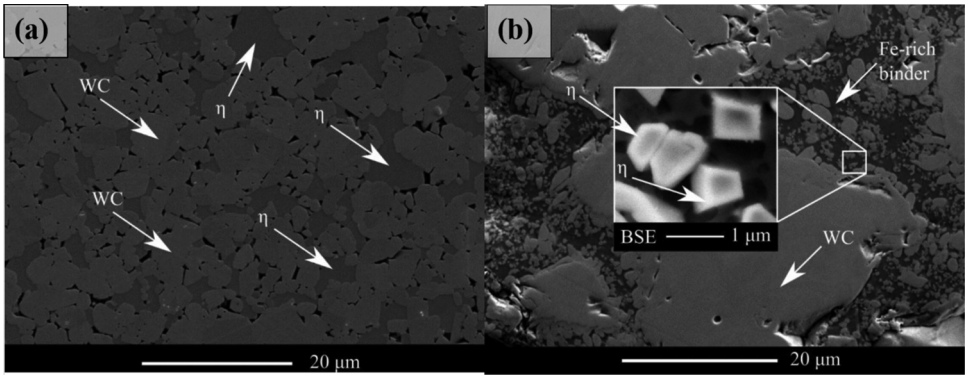

Fig. 14. SEM micrographs of WC-SS: (a) conventionally sintered; (b) SLS manufactured [59].

(CTE) of the matrix and phase transition from FCC to BCC in the matrix.

In terms of dimensional accuracy, due to the adhesion of the powder to the built-up edge dimensions may increase. When the process parameters are optimized for the bulk they may not result in the proper quality for the boundary area. Kumar and Czekanski [58] reported that due to the powder adherence phenomenon the diameter of a pin increases while that of a hole decreases.

2.3. Laser engineered net shaping (LENS)

Laser engineered net shaping (LENS) is another process that is used for the production of cermet components. In this process, the material powder is injected into a molten pool on the surface of a solid substrate created by a high-powered laser beam. LENS is known not only as a process for fabricating complex geometries but also as a surface treatment process [88]. The effective process parameters in the LENS process that significantly affect the profiles and microstructures are laser power, powder feed rate, traverse speed, and working distance (see Fig. 15). For instance, a larger layer thickness can be achieved by increasing the laser power or powder feed rate, or by decreasing the traverse speed. Short working distance leads to a slight increase in sample density and enhanced microstructure uniformity [62]. Xiong and et al. [61] reported that depending on the position along the height of the LENS samples, different mechanical properties can be obtained. This difference in mechanical properties is due to the change in the cooling rate along with the height of the specimen. Lower hardness was reported at layers close to the top surface of WC-10 % Co cermets which was attributed to the variation of cooling rate along the longitudinal section. Besides, it has been stated that optimized process parameters result in the production of dense and crack-free thin wall specimens.

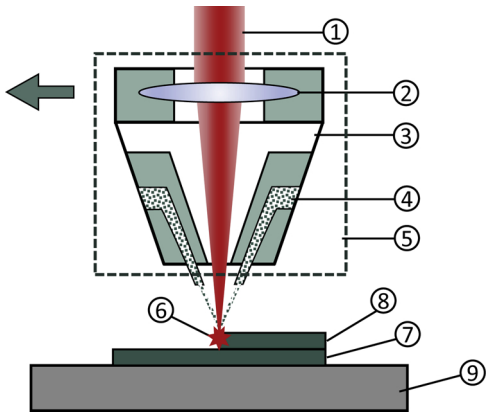

Fig. 15. Schematic illustration of the LENS process: (1) laser beam, (2) focusing lens, (3) shield gas, (4) powder stream, (5) deposition head, (6) molten pool, (7) 1st deposited layer, (8) layer being deposited, and (9) build platform.

With regard to the microstructure Xiong et al. [61,62] reported a gradient of dark to bright layer in the manufactured WC-10 %Co sample (Fig. 16). High magnification analysis of the sample shown in Fig.16 revealed that the boundary area between two deposited layers consists of fine WC particles (smaller than 100 nm) in the darker region and large WC particles (submicron or micron scale) in the brighter side, formed due to grain growth in the binder phase.

In another research by Xiong et al. [63], the influence of laser power, powder feed rate and transverse speed on layer thickness was verified by specimen height. The experimental results showed that increasing the laser power and powder feed as well as decreasing the transverse speed results in higher sample heights (Fig. 17).

Xiong et al. [63] reported that during the production of (Ti,W)C–Ni cermet by the LENS process, the concentration of Ni decreases due to the evaporation of Ni during the process. Moreover, the typical core/rim microstructure which is usually observed in conventional cermets was not reported by these researchers. It has also been reported that producing (Ti,W)C–Ni cermet with maximum density by the LENS process is more difficult than producing WC-Co with maximum density because the wettability of TiC and WC by Ni is weaker than that of WC by Co. In addition, the high hardness of components fabricated by LENS can be attributed to the high concentration of the (Ti,W)C phase compared to conventional processes. The LENS process also results in inhomogeneous microstructure and grain coarsening.

2.4. Direct laser fabrication (DLF)

Direct laser fabrication is another promising method to manufacture 3D samples of advance materials layer by layer with direct deposition of powders in a melt pool. In-situ production of TiC-(20, 30, 40 Vol%)Ni cermet by direct laser fabrication (DLF) has been investigated [64]. It was shown that with increasing Ni content, the bending strength and hardness of the manufactured samples decreased. This was attributed to the reduction of the ceramic phase fraction with increasing Ni binder (Fig.18).

As shown in Fig. 19, Ni content can also affect the microstructure of the fabricated TiC-Ni cermets. By increasing the Ni content (grey phase) the size of TiC particles (dark black round shape phase) decreases. It is supposed that increasing Ni as a diluent can reduce the temperature rise due to the exothermic reaction between Ti and C. Furthermore, TiC particles can be surrounded by molten binder when using higher Ni content reducing the TiC grain growth.

2.5. Binder jet 3D printing

Binder jet 3D printing is another process that has been used for WC-12 %Co production [66–68]. This process is one of the AM processes with the potential to produce cemented carbide parts of complex geometry. Two kinds of materials are used in binder jet 3D printing, which

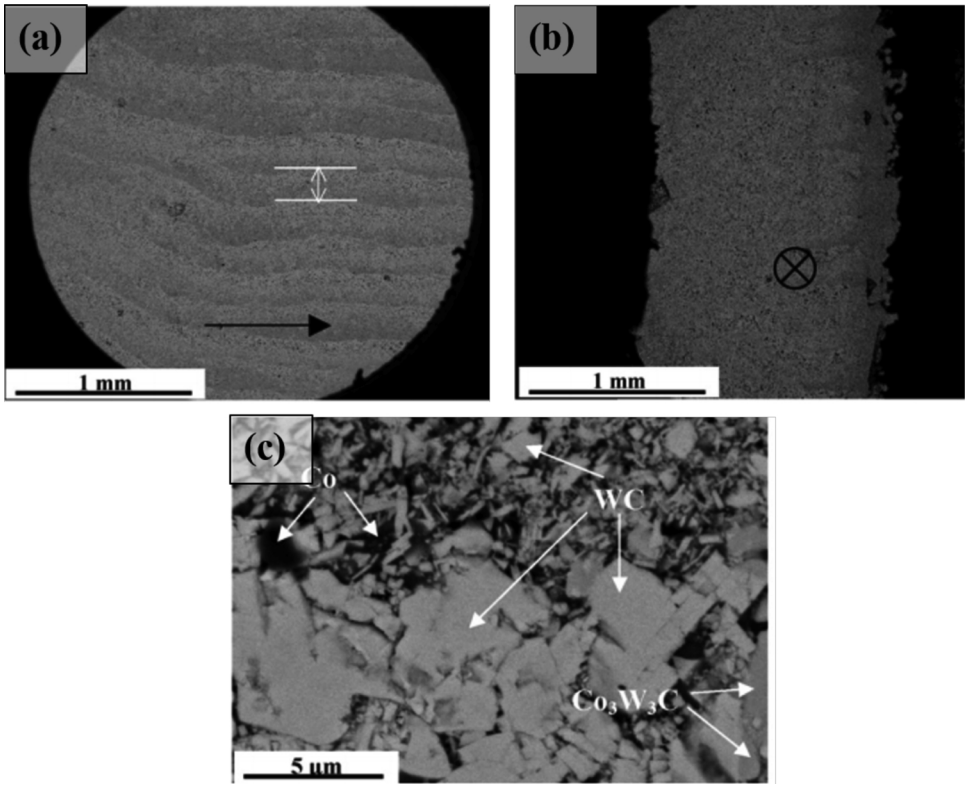

Fig. 16. SEM(BSE) images of a LENS WC–Co thin wall specimen fabricated using a laser power of 200 W: (a) side view image representing the alternating layers; (b) cross-sectional view (the circle with a cross illustrates the deposition direction, perpendicular to the section); (c) high magnification image of (a) showing details of the boundary area between the sintered layers [62].

are powder and binder. The binder is in liquid form and acts as an adhesive film bonding the powder layer at low temperatures. Similar to the laser-based processes, in which the laser scanning pattern follows the slides of the component geometry, the same method is used for the deposition of the binder on top of the powder bed (see Fig. 20). Printed parts are heated to 2000 °C followed by sintering, in order to cure the binder and improve the strength. The main disadvantages of binder jet printing are volume change of specimens from the green to fully consolidated parts and the necessity of extensive post-processing to remove the binder which leads to shrinkage and distortion of samples. The infiltration of porous specimens is a possible solution to solve these problems. This compromises the strength and design of the final components [32,89].

Enneti and Prough [32] investigated the wear behavior of WC-12 %Co cermet manufactured by binder jet 3D printing. Binder jet 3D printed cermet showed lower volume loss in comparison with

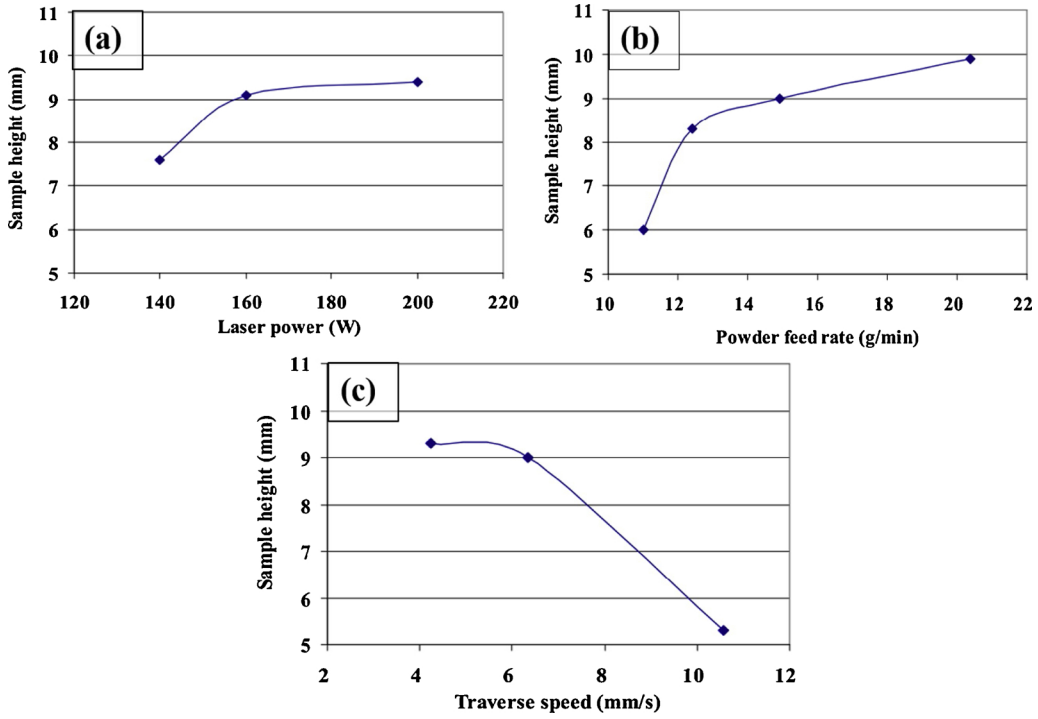

Fig. 17. Effect of variation of (a) laser power, (b) powder feed, and (c) transverse speed on sample height [61].

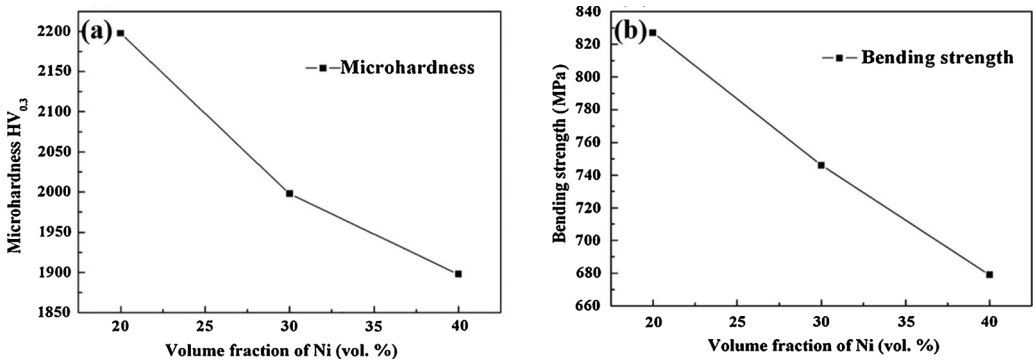

Fig. 18. Effect of Ni volume fraction on, (a) microhardness, and (b) bending strength of TiC-Ni [64].

conventionally produced cemented carbides [90]. They attributed superior wear resistance to the dual grain size microstructure of the WC in the sintered BJ3DP material as seen in Fig. 21.

Post infiltration of binder jet 3D printed components with a molten metal can be used for manufacturing cemented carbides. This approach involves printing, debonding and sintering of carbide parts followed by infiltration with the metallic binder. A number of studies showed that by using this approach nearly full density with high hardness and fracture toughness comparable with conventional cermets can be achieved. However, even with using post infiltration, some of the additive manufacturing challenges such as cracks, porosities and shrinkage are not avoidable [71–74] Fig. 22.

2.6. Extrusion-Based 3D-Printing

Recently extrusion-based 3D-printing has been developed for the production of hardmetals and cermets using SDS (shaping–debinding–sintering) process. In this technique the feedstock can be a wire or granulated powder which are called fused-filament fabrication (FFF) and composite-extrusion modeling (CEM), respectively. In both methods the feedstock is fused and the free-form is printed through a nozzle [75].

Lengauer et al. [33] and Michael et al. [69] produced (WC-10 %Co) hardmetal and (Ti(C,N), WC,(Ta,Nb)C, Cr_3C_2)-Co, Ni cermet by FFF method and WC-Co by CEM process. Although The obtained microstructure was similar to the conventionally manufactured parts, full density was not reached, the roughness of the surface was high and the samples had porosities between the layers. The lack of quality emerged due to lack of process parameter optimization.

2.7. 3D gel-printing (3DGP)

Since the production of WC-20Co by most AM processes is complicated and has a number of limitations, recently, a new AM process, known as 3D gel-printing (3DGP), has been developed [91]. By combining the concepts of material extrusion and conventional casting, 3DGP is able to transform the 3D model into a 3D entity. In this technique, a slurry of powder in a solution of organic monomers (also known as ink) is delivered to a screw extruder at specific compressed air pressure. In the meantime, an initiator and a catalyst are proportionally injected to the same screw extruder, blended, extruded, and then deposited layer by layer on the build platform. After a short time, the organic monomer polymerizes, and the solid powder is fixed *in situ* by the 3D cross-linked polymers (known as a green body) [34]. (see Fig.23)

It has been reported [34] that the density of green and sintered samples (sintered at 1360 °C for 1 h in the vacuum in a carbon tube furnace, vacuum < 2 Pa) produced by 3DGP increases by increasing the solid loading in the slurry (Fig. 24). It is worth mentioning that if the green density of the sample increases, shrinkage of the part during the sintering process will be decreased which means more dimensional accuracy in sintered material can be attained. According to SEM

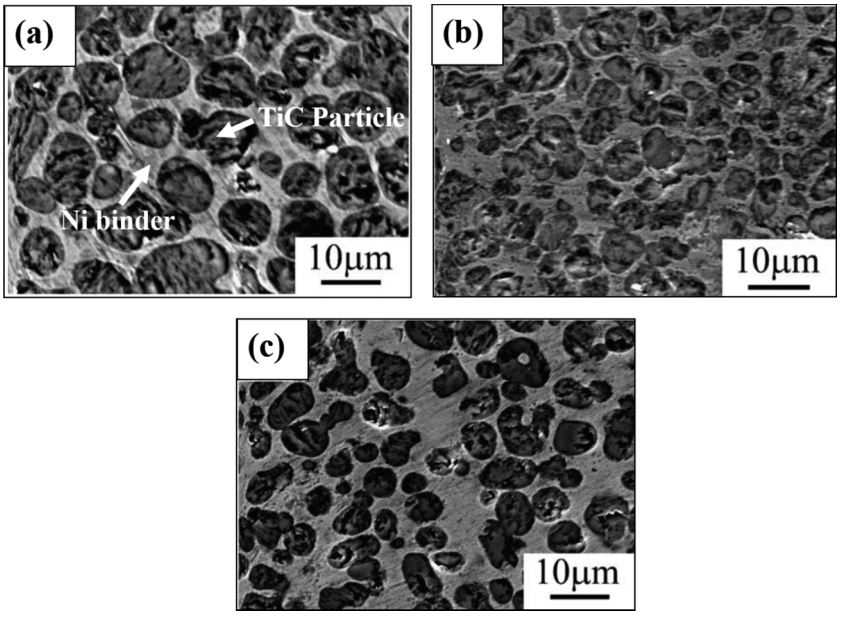

Fig. 19. SEM micrographs of the TiC–Ni cermet prepared by DLF (a) 20, (b) 30 and (c) 40 vol.% Ni [64].

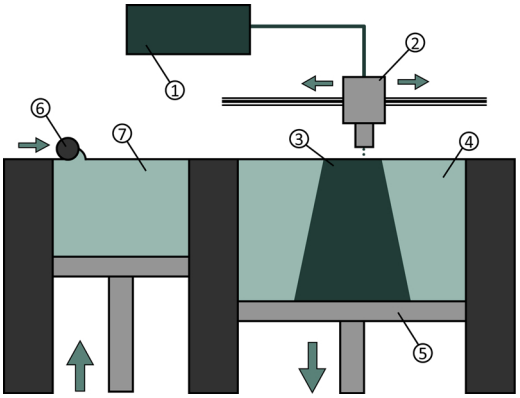

Fig. 20. Schematic illustration of Binder jet 3D printing process: (1) liquid binder, (2) inkjet print head, (3) printed object, (4) powder bed, (5) build platform, (6) powder roller, and (7) new powder stock.

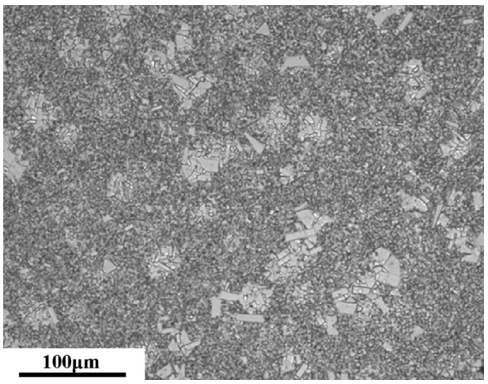

Fig. 21. The sintered microstructure of the WC-12 %Co showing dual grain size [32].

analysis of 3DGP samples increasing the solid loading reduces the internal porosity (Fig. 25). Zhang et al. [34] were able to fabricate cermets of 99.93 % density using the proper solid loading during the fabrication of cermets by 3DGP. The lower the solid loading, the higher is the amount of solvent and organic binder in 3DGP samples. The high content of the solvent and organic bonder leads to the formation of more porosity in the samples during the debonding and sintering.

As presented in Fig. 26 increasing the solid loading can enhance the hardness and transverse rupture strength of sintered 3DGP samples. This finding was indicated by the lower density of the samples with lower solid content than those with higher solid content [34].

Fig. 27 represents a bevel milling cutter produced by the 3DGP process. Despite the high density of the produced component, tracks of printing layers can be seen on the surface of the component. Surface treatment methods such as polishing and finishing are needed in this case to fulfill the requirements of the part for real-life applications.

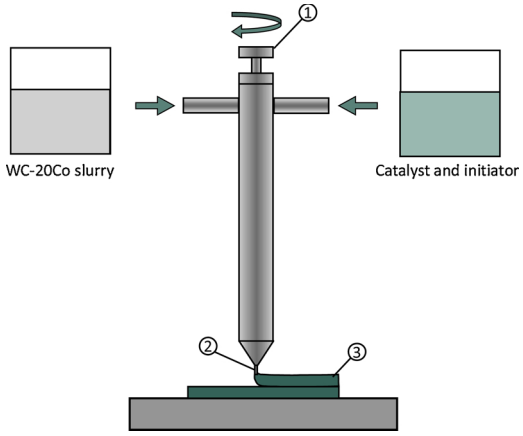

Fig. 23. Schematic illustration of 3D gel-printing process: (1) screw extruder, (2) nozzle, and (3) green body.

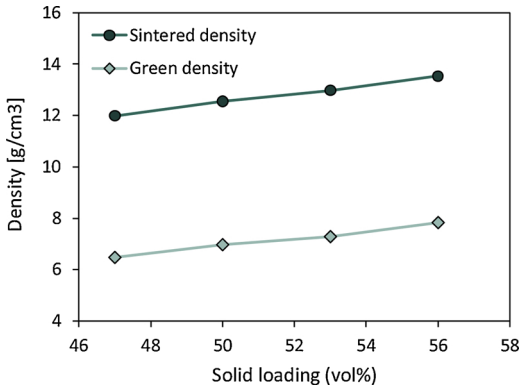

Fig. 24. Green and sintered densities of 3DGP samples with different WC-20Co solid loadings [34].

3. Outlook and conclusion

Undoubtedly, AM has received extensive attention in recent years and the range of materials that can be printed by these processes has increased rapidly. However, the AM technique has mainly been developed and commercialized for polymeric and metallic structural parts and controlling process parameters for the production of ceramics and ceramic-based materials; in particular, cermets is still challenging. During the last few years, different kinds of AM processes such as SLM, SLS, LENS, DLF, Binder jet 3D printing,Extrusion-based 3D-printing, and 3D gel/direct-ink-write/robocasting printing have been used for the fabrication of cermets, in particular, hard metals (WC-Co). For this aim, different process parameters and chemical compositions have been studied by researchers in order to obtain AM cermet parts of appropriate mechanical properties.

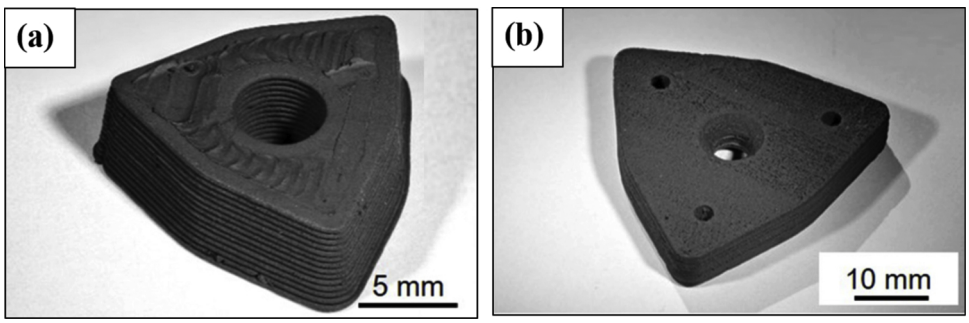

Fig. 22. Specimens manufactured by (a) FFF, and (b) CEM process [33].

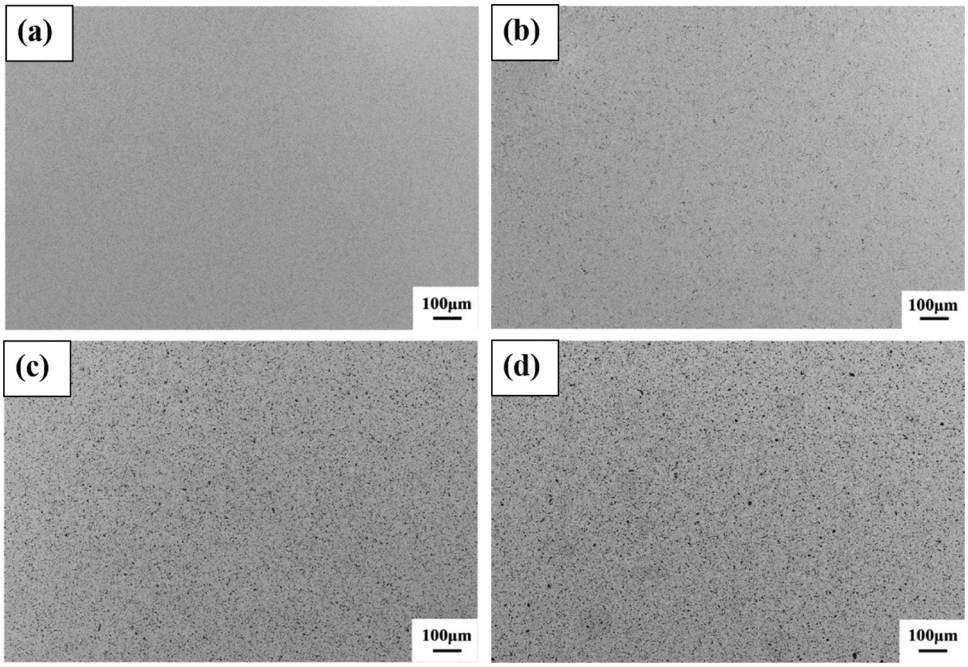

Fig. 25. SEM images of sintered samples printed by 3DGP using WC-20Co slurries with different solid loading: (a) 56 vol%, (b) 53 vol%, (c) 50 vol%, and (d) 47 vol% [34].

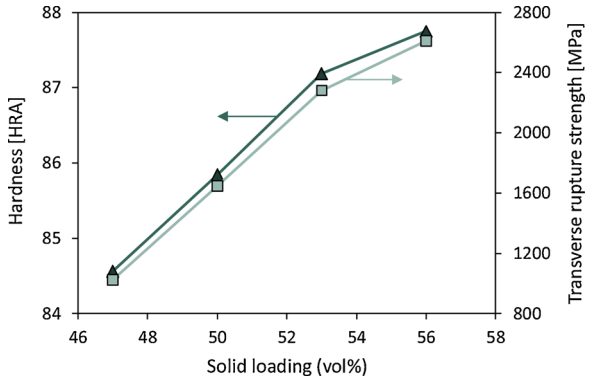

Fig. 26. Hardness values and bending strength for sintered 3DGP samples with various WC-20Co solid loadings [34].

In terms of SLS/SLM, which includes the majority of research in the field of AM manufacturing of cermets and hard metals, various powder preparation processes, material compositions and process parameters have been surveyed. The milling process of the powder mixture and surface modification processes such as chemical vapor deposition (CVD), sputtering cold spray, etc. are the common powder preparation processes. In some cases such as; SLM [39,42] and SLS [30,41] scholars reported successful fabrication with relatively acceptable quality. Different values of the microhardness were reported for fabricated parts, which were directly affected by the chemical composition, grain size, porosity and internal defects in the specimens. The common microstructure formation mechanism in SLS/SLM processes is as follows: melting of a low melting point phase (metal phase), wetting of the surface of ceramic particles with molten metal, surface tension and consequently Marangoni effect due to high-temperature gradient between center to edge of melt pool which induces capillarity force for liquid flow and particle rearrangement and subsequently, uniform

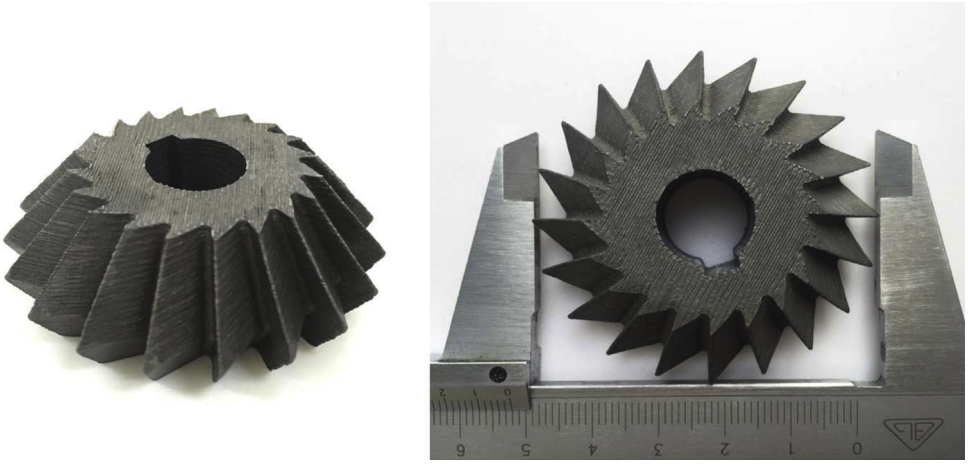

Fig. 27. A bevel milling cutter (52 mm in diameter) produced by 3DGP and sintered at 1360 °C [34].

distribution of the liquid metal between the ceramic particles.

Dealing with other AM processes, successful fabrication of cermet samples with acceptable qualities was reported in several types of research on LENS [54], DLF [57], Binder jet printing [32] and 3DGP [33] processes. Despite the efforts for maximizing the quality of the final product, microcracking, porosity, and lack of geometrical accuracy in manufactured parts using laser-based techniques are still considered as the main challenges. On the other hand, cermet components produced by binder jet printing and 3DGP seem to give a limited amount of internal porosity with a relatively high density near to the theoretical density. Despite small amounts of internal porosity in the components produced by these techniques, the requirement of high-temperature post sintering of these parts in a vacuum environment may not always be applicable and would increase the cost of fabrication process compared to the other laser-based techniques. Additionally, a coarser staircase effect and waviness of the surface in 3DGP parts due to relatively large layer height can be considered as a drawback for this process. Hence, producing cermets and achieving optimized process parameters to manufacture these materials with higher density and acceptable surface morphology requires additional investigation. Moreover, there is limited information about the mechanical, wear, and corrosion properties of cermets fabricated by AM techniques, compared to those produced by conventional methods. Therefore, there is a significant potential for research in this field to achieve optimal fabrication parameters resulting in favorable properties. There is no clear understanding of the relationship between process parameters, the resultant microstructures, and the mechanical behavior of cermets fabricated by AM techniques. Also, an optimal build strategy for in-situ fabrication of cermets with minimal internal defects and controlled residual stresses is yet to be determined.

Various methods can be employed to further control the favorable phases after AM production of cermets. Applicability of different post-processing techniques such as hot isostatic pressing (HIP), sandblasting, shot peening, chemical etching, heat treatment, etc., on AM cermets to improve their mechanical performance might be considered as potential research topics in this field. Although the possibility of producing cermet components with simple geometries using different AM technologies has been the topic of the available articles in the open literature, thus far, no research has been conducted to produce cermet components of geometries appropriate for real-life applications. Given the fact that AM methods are mainly being used to produce components with complex geometries, microstructural features, and structural behavior of AM cermet components with geometrical discontinuities should be studied. The current challenges in fabrication and characterization of this type of material will undoubtedly be overcome, and a sound future for the production and application of AM cermet components is anticipated.

Funding

This research did not receive any specific grant from funding agencies in the public, commercial, or not-for-profit sectors.

Declaration of Competing Interest

None.

References

[1] S. Buchholz, Z.N. Farhat, G.J. Kipouros, K.P. Plucknett, The reciprocating wear behaviour of TiC–Ni3Al cermets, Int. J. Refract. Met. Hard Mater. 33 (2012) 44–52, https://doi.org/10.1016/J.IJRMHM.2012.02.008.

[2] L. Jaworska, M. Rozmus, B. Królicka, A. Twardowska, Functionally graded cermets, J. Achiev. Mater. Manuf. Eng. 17 (2006) 73–76.

[3] B.G. Compton, F.W. Zok, Impact resistance of TiC-based cermets, Int. J. Impact Eng. 62 (2013) 75–87, https://doi.org/10.1016/j.ijimpeng.2013.06.008.

[4] E.G. Pickering, M.R. O'Masta, H.N.G. Wadley, V.S. Deshpande, Effect of confinement on the static and dynamic indentation response of model ceramic and cermet materials, Int. J. Impact Eng. 110 (2016), https://doi.org/10.1016/j.ijimpeng.2016.12.007.

[5] C. Han, M. Kong, Fabrication and properties of TiC-based cermet with intra /intergranular microstructure, Mater. Des. 30 (2009) 1205–1208, https://doi.org/10.1016/j.matdes.2008.06.019.

[6] A. Rajabi, M.J. Ghazali, A.R. Daud, Chemical composition, microstructure and sintering temperature modifications on mechanical properties of TiC-based cermet – a review, J. Mater. 67 (2015) 95–106, https://doi.org/10.1016/j.matdes.2014.10.081.

[7] P. Alvaredo, D. Mari, E. Gordo, High temperature transformations in a steel-TiCN cermet, Int. J. Refract. Met. Hard Mater. 41 (2013) 115–120, https://doi.org/10.1016/j.ijrmhm.2013.02.012.

[8] Z. Guo, J. Xiong, M. Yang, C. Jiang, WC – TiC – Ni cemented carbide with enhanced properties, J. Alloys. Compd. 465 (2008) 157–162, https://doi.org/10.1016/j.jallcom.2007.10.132.

[9] I. Hussainova, Some aspects of solid particle Erosion of cermets, Tribol. Int. 34 (2001) 89–93, https://doi.org/10.1016/S0301-679X(00)00140-7.

[10] W. Lengauer, The Story of Cermets, (2016).

[11] M. Razavi, M.S. Yaghmaee, M.R. Rahimipour, S.S. Razavi Tousi, The effect of production method on properties of Fe-TiC composite, Int. J. Miner. Process. 94 (2010) 97–100, https://doi.org/10.1016/j.minpro.2010.01.002.

[12] A. Jam, L. Nikzad, M. Razavi, TiC-based cermet prepared by high-energy ball-milling and reactive spark plasma sintering, Ceram. Int. 43 (2017) 2448–2455, https://doi.org/10.1016/j.ceramint.2016.11.039.

[13] J. Park, S. Hong, M. Lee, C. Rhee, Effects of metal additions on refinement behavior of TiC particles during a very high speed milling process, Powder Technol. 249 (2013) 126–133, https://doi.org/10.1016/j.powtec.2013.07.006.

[14] F. Akhtar, S.J. Askari, J.A. Shah, S. Guo, Processing, microstructure and mechanical properties of TiC-465 stainless steel/465 stainless steel layer composites, J. Alloys. Compd. 439 (2007) 287–293, https://doi.org/10.1016/j.jallcom.2006.08.073.

[15] R. Hasniyati, H. Zuhailawati, S. Ramakrishnan, Mechanism and optimization of titanium carbide-reinforced iron composite formation through carbothermal reduction of hematite and anatase, J. Alloys. Compd. 587 (2014) 442–450, https://doi.org/10.1016/j.jallcom.2013.10.245.

[16] W. Zhang, X. Zhang, J. Wang, C. Hong, Effect of Fe on the phases and microstructure of TiC – Fe cermets by combustion synthesis / quasi-isostatic pressing, Mater. Sci. Eng., A 381 (2004) 92–97, https://doi.org/10.1016/j.msea.2004.04.026.

[17] D.H. Bacon, L. Edwards, J.E. Moffatt, M.E. Fitzpatrick, Fatigue and fracture of a 316 stainless steel metal matrix composite reinforced with 25 % titanium diboride, Int. J. Fatigue 48 (2013) 39–47, https://doi.org/10.1016/j.ijfatigue.2012.09.016.

[18] F. Akhtar, S.J. Guo, Microstructure, mechanical and fretting wear properties of TiC-stainless steel composites, Mater. Charact. 59 (2008) 84–90, https://doi.org/10.1016/j.matchar.2006.10.021.

[19] B. Li, Y. Liu, J. Li, H. Cao, L. He, Effect of sintering process on the microstructures and properties of in situ TiB 2 – TiC reinforced steel matrix composites produced by spark plasma sintering, J. Mater. Process. Technol. 210 (2010) 91–95, https://doi.org/10.1016/j.jmatprotec.2009.08.008.

[20] R. Ohser-wiedemann, C. Weck, U. Martin, A. Müller, H.J. Seifert, Spark plasma sintering of TiC particle-reinforced molybdenum composites, Int. J. Refract. Met. Hard Mater. 32 (2012) 1–6, https://doi.org/10.1016/j.ijrmhm.2011.12.001.

[21] Y.F. Yang, H.Y. Wang, R.Y. Zhao, Y.H. Liang, L. Zhan, Q.C. Jiang, Effects of C particle size on the ignition and combustion characteristics of the SHS reaction in the 20 wt. % Ni–Ti–C system, J. Alloys. Compd. 460 (2008) 276–282, https://doi.org/10.1016/j.jallcom.2007.06.010.

[22] H. Kwon, C. Suh, W. Kim, Microstructure and mechanical properties of (Ti, W) C – Ni cermet prepared using a nano-sized TiC – WC powder mixture, J. Alloys. Compd. 639 (2015) 21–26, https://doi.org/10.1016/j.jallcom.2015.03.115.

[23] A. Khalili, M. Goodarzi, M. Mojtahedi, M. Javad, Solidification microstructure of in-situ laser-synthesized Fe-TiC hard coating, Surf. Coat. Technol. 307 (2016) 747–752, https://doi.org/10.1016/j.surfcoat.2016.09.051.

[24] K.J.A. Brookes, 3D-printing style additive manufacturing for commercial hardmetals, Met. Powder Rep. 70 (2015) 137–140, https://doi.org/10.1016/j.mprp.2015.04.011.

[25] J.C. Ruiz-Morales, Three dimensional printing of components and functional devices for energy and environmental applications, Energy Environ. Sci. 10 (2017) 846–859, https://doi.org/10.1039/c6ee03526d.

[26] K.V. Wong, A. Hernandez, "A review of additive manufacturing,", ISRN Mech. Eng. (2012) 1–10, https://doi.org/10.5402/2012/208760.

[27] F.E. Wiria, B.Y. Tay, Direct selective laser sintering and melting of ceramics: a review, Rapid Prototyp. J. (2017), https://doi.org/10.1108/RPJ-11-2015-0178.

[28] D. Dai, D. Gu, H. Zhang, J. Xiong, C. Ma, C. Hong, Influence of scan strategy and molten pool configuration on microstructures and tensile properties of selective laser melting additive manufactured aluminum based parts, Opt. Laser Technol. 99 (2018) 91–100, https://doi.org/10.1016/j.optlastec.2017.08.015.

[29] E. Uhlmann, A. Bergmann, W. Gridin, Investigation on additive manufacturing of tungsten carbide-cobalt by selective laser melting, Procedia Cirp 35 (2015) 8–15, https://doi.org/10.1016/j.procir.2015.08.060.

[30] D. Gu, Y. Shen, Direct laser sintered WC-10Co/Cu nanocomposites, Appl. Surf. Sci. 254 (2008) 3971–3978, https://doi.org/10.1016/j.apsusc.2007.12.028.

[31] Y. Xiong, J.E. Smugeresky, E. Lavernia, J.M. Schoenung, Processing and microstructure of WC-CO cermets by laser engineered net shaping, 19th Annu. Int. Solid Free. Fabr. Symp, SFF 2008, 2008.

[32] R.K. Enneti, K.C. Prough, Wear properties of sintered WC-12%Co processed via Binder Jet 3D Printing (BJ3DP), Int. J. Refract. Met. Hard Mater. 78 (2019)

228–232, https://doi.org/10.1016/j.ijrmhm.2018.10.003.
[33] W. Lengauer, I. Duretek, M. Fürst, V. Schwarz, J. Gonzalez-Gutierrez, S. Schuschnigg, C. Kukla, M. Kitzmantel, E. Neubauer, C. Lieberwirth, V. Morrison, Fabrication and properties of extrusion-based 3D-printed hardmetal and cermet components, Int. J. Refract. Met. Hard Mater. 82 (2019) 141–149, https://doi.org/10.1016/j.ijrmhm.2019.04.011.
[34] X. Zhang, Z. Guo, C. Chen, W. Yang, Additive manufacturing of WC-20Co components by 3D gel-printing, Int. J. Refract. Met. Hard Mater. 70 (2018) 215–223, https://doi.org/10.1016/j.ijrmhm.2017.10.005.
[35] P. Krakhmalev, I. Yadroitsev, Microstructure and properties of intermetallic composite coatings fabricated by selective laser melting of Ti-SiC powder mixtures, Intermetallics. 46 (2014) 147–155, https://doi.org/10.1016/j.intermet.2013.11.012.
[36] M. Horn, P. Regenfuß, H. Exner, Bodies of cermet-like materials by laser micro sintering, 18th Plansee Semin. (2013) 1–10.
[37] K. Maeda, T.H.C. Childs, Laser sintering (SLS) of hard metal powders for abrasion resistant coatings, J. Mater. Process. Technol. 149 (2004) 609–615, https://doi.org/10.1016/j.jmatprotec.2004.02.024.
[38] V.K. Balla, S. Bose, A. Bandyopadhyay, Microstructure and wear properties of laser deposited WC-12%Co composites, Mater. Sci. Eng. A. 527 (2010) 6677–6682, https://doi.org/10.1016/j.msea.2010.07.006.
[39] J.A. Picas, Y. Xiong, M. Punset, L. Ajdelsztajn, A. Forn, J.M. Schoenung, Microstructure and wear resistance of WC-Co by three consolidation processing techniques, Int. J. Refract. Met. Hard Mater. 27 (2009) 344–349, https://doi.org/10.1016/j.ijrmhm.2008.07.002.
[40] D. Gu, W. Meiners, Microstructure characteristics and formation mechanisms of in situ WC cemented carbide based hard metals prepared by Selective Laser Melting, Mater. Sci. Eng. A. 527 (2010) 7585–7592, https://doi.org/10.1016/j.msea.2010.08.075.
[41] A. Davydova, A. Domashenkov, A. Sova, I. Movtchan, P. Bertrand, B. Desplanques, N. Peillon, S. Saunier, C. Desrayaud, S. Bucher, C. Iacob, Selective laser melting of boron carbide particles coated by a cobalt-based metal layer, J. Mater. Process. Technol. 229 (2016) 361–366, https://doi.org/10.1016/j.jmatprotec.2015.09.033.
[42] A. Domashenkov, A. Borbély, I. Smurov, Structural modifications of WC/Co nanophased and conventional powders processed by selective laser melting, Mater. Manuf. Process. 32 (2016) 93–100, https://doi.org/10.1080/10426914.2016.1176195.
[43] R.S. Khmyrov, V.A. Safronov, A.V. Gusarov, Synthesis of nanostructured WC-Co hardmetal by selective laser melting, Procedia IUTAM 23 (2017) 114–119, https://doi.org/10.1016/j.piutam.2017.06.011.
[44] R.S. Khmyrov, A.P. Shevchukov, A.V. Gusarov, T.V. Tarasova, Phase composition and microstructure of WC-Co alloys obtained by selective laser melting, Mech. Ind. 18 (2017), https://doi.org/10.1051/meca/2017059.
[45] S. Grigoriev, T. Tarasova, A. Gusarov, R. Khmyrov, S. Egorov, Possibilities of manufacturing products from cermet compositions using nanoscale powders by additive manufacturing methods, Materials (Basel). 12 (2019), https://doi.org/10.3390/ma12203425.
[46] J. Chen, M. Huang, Z.Z. Fang, M. Koopman, W. Liu, X. Deng, Z. Zhao, S. Chen, S. Wu, J. Liu, W. Qi, Z. Wang, Microstructure analysis of high density WC-Co composite prepared by one step selective laser melting, Int. J. Refract. Met. Hard Mater. 84 (2019) 104980, , https://doi.org/10.1016/j.ijrmhm.2019.104980.
[47] S.L. Campanelli, N. Contuzzi, P. Posa, A. Angelastro, Printability and microstructure of selective laser melting of WC/Co/Cr powder, Materials (Basel). 12 (2019), https://doi.org/10.3390/ma12152397.
[48] X.C. Wang, T. Laoui, J. Bonse, J.P. Kruth, B. Lauwers, L. Froyen, Direct selective laser sintering of hard metal powders: experimental study and simulation, Int. J. Adv. Manuf. Technol. 19 (2002) 351–357, https://doi.org/10.1007/s001700200024.
[49] D.D. Gu, Y.F. Shen, P. Dai, M.C. Yang, Microstructure and property of sub-micro WC-10%Co particulate reinforced Cu matrix composites prepared by selective laser sintering, Trans. Nonferrous Met. Soc. China (English Ed. 16 (2006) 357–362, https://doi.org/10.1016/S1003-6326(06)60061-7.
[50] D. Gu, Y. Shen, WC-Co particulate reinforcing Cu matrix composites produced by direct laser sintering, Mater. Lett. 60 (2006) 3664–3668, https://doi.org/10.1016/j.matlet.2006.03.103.
[51] A. Gåård, P. Krakhmalev, J. Bergström, Microstructural characterization and wear behavior of (Fe,Ni)-TiC MMC prepared by DMLS, J. Alloys. Compd. 421 (2006) 166–171, https://doi.org/10.1016/j.jallcom.2005.09.084.
[52] D. Gu, Y. Shen, L. Zhao, J. Xiao, P. Wu, Y. Zhu, Effect of rare earth oxide addition on microstructures of ultra-fine WC-Co particulate reinforced Cu matrix composites prepared by direct laser sintering, Mater. Sci. Eng. A. 445–446 (2007) 316–322, https://doi.org/10.1016/j.msea.2006.09.057.
[53] L.F.S. Kumar, J.-P. Kruth, Wear behaviour of SLS WC-Co composites, Proc. Solid Free. Fabr. Symp, Austin, Texas, 2008.
[54] S. Kumar, Manufacturing of WC-Co moulds using SLS machine, J. Mater. Proc. IEEE Int. Symp. Signal Proc. Inf. Tech. 209 (2009) 3840–3848, https://doi.org/10.1016/j.jmatprotec.2008.08.037.
[55] C.N. Sun, T. Baldridge, M.C. Gupta, Fabrication of ZrB2-Zr cermet using laser sintering technique, Mater. Lett. 63 (2009) 2529–2531, https://doi.org/10.1016/j.matlet.2009.08.059.
[56] H. Kyogoku, T. Uemori, A. Ikuta, K. Yoshikawa, H. Ohmori, Proceedings of the ASME/ISCIE 2012 International Symposium on Flexible Automation ISFA2012 June 18-20, 2012, St. Louis, Missouri, USA, 2012, pp. 18–21.
[57] A. Filippov, V.M. Fomin, A. Malikov, A. Orishich, Selective laser sintering of cermet mixtures Ti and B4C, Int. Conf. Methods Aerophysical Res. (ICMAR 2016) AIP (2016) 30095, https://doi.org/10.1063/1.4964037.
[58] S. Kumar, A. Czekanski, Optimization of parameters for SLS of WC-Co, Rapid Prototyp. J. 23 (2017) 1202–1211, https://doi.org/10.1108/RPJ-10-2016-0168.
[59] A.J. Cavaleiro, C.M. Fernandes, A.R. Farinha, C.V. Gestel, J. Jhabvala, E. Boillat, A.M.R. Senos, M.T. Vieira, The role of nanocrystalline binder metallic coating into WC after additive manufacturing, Appl. Surf. Sci. 427 (2018) 131–138, https://doi.org/10.1016/j.apsusc.2017.08.039.
[60] S. Kumar, Process chain development for additive manufacturing of cemented carbide, J. Manuf. Process. 34 (2018) 121–130, https://doi.org/10.1016/j.jmapro.2018.05.036.
[61] Y. Xiong, J.E. Smugeresky, L. Ajdelsztajn, J.M. Schoenung, Processing and Microstructure of WC-Co cermets by laser engineering net shaping, Mater. Sci. Eng. A. 493 (2008) 261–266, https://doi.org/10.1016/j.msea.2007.05.125.
[62] Y. Xiong, J.E. Smugeresky, J.M. Schoenung, The influence of working distance on laser deposited WC-Co, J. Mater. Process. Technol. 209 (2009) 4935–4941, https://doi.org/10.1016/j.jmatprotec.2009.01.016.
[63] Y. Xiong, M. Kim, O. Seo, J.M. Schoenung, S. Kang, (Ti,W)C–Ni cermets by laser engineered net shaping, Powder Metall. 53 (2010) 41–46, https://doi.org/10.1179/174329009x380581.
[64] Y. Li, P. Bai, Y. Wang, J. Hu, Z. Guo, Effect of Ni contents on the microstructure and mechanical properties of TiC-Ni cermets obtained by direct laser fabrication, Int. J. Refract. Met. Hard Mater. 27 (2009) 552–555, https://doi.org/10.1016/j.ijrmhm.2008.07.006.
[65] B.D. Kernan, E.M. Sachs, M.A. Oliveira, M.J. Cima, Three-dimensional printing of tungsten carbide-10 wt% cobalt using a cobalt oxide precursor, Int. J. Refract. Met. Hard Mater. 25 (2007) 82–94, https://doi.org/10.1016/j.ijrmhm.2006.02.002.
[66] P. Paul D, G.B. Collins, Cemented carbide powders for additive manufacturing, U.S. Patent Application 15 (437) (2018) 153.
[67] R.K. Enneti, K.C. Prough, International Journal of Refractory Metals E ff ect of binder saturation and powder layer thickness on the green strength of the binder jet 3D printing (BJ3DP) WC-12 % Co powders, Int. J. Refract. Metals Hard Mater. 84 (2019) 104991, , https://doi.org/10.1016/j.ijrmhm.2019.104991.
[68] J.D. Flon, Three dimensional printing of cermet or cemented carbide, U.S. Patent Application 16 (093) (2019) 554.
[69] K. Michael, L. Walter, D. Ivica, S. Viktoria, Potential of extrusion based 3D-printed hardmetal and cermet parts, World Congr. Powder Metall. (2018).
[70] U. Scheithauer, J. Pötschke, S. Weingarten, E. Schwarzer, A. Vornberger, T. Moritz, A. Michaelis, Droplet-based additive manufacturing of hard metal components by thermoplastic 3D Printing (T3DP), J. Ceram. Sci. Technol. 8 (2017) 155–160, https://doi.org/10.4416/JCST2016-00104.
[71] C.L. Cramer, T.G. Aguirre, N.R. Wieber, R.A. Lowden, A.A. Trofimov, H. Wang, J. Yan, M.P. Paranthaman, A.M. Elliott, Binder jet printed WC infiltrated with premade melt of WC and Co, Int. J. Refract. Met. Hard Mater. (2019) 105137, , https://doi.org/10.1016/j.ijrmhm.2019.105137.
[72] C.L. Cramer, P. Nandwana, R.A. Lowden, A.M. Elliott, Infiltration studies of additive manufacture of WC with Co using binder jetting and pressureless melt method, Addit. Manuf. 28 (2019) 333–343, https://doi.org/10.1016/j.addma.2019.04.009.
[73] C.L. Cramer, N.R. Wieber, T.G. Aguirre, R.A. Lowden, A.M. Elliott, Shape retention and infiltration height in complex WC-Co parts made via binder jet of WC with subsequent Co melt infiltration, Addit. Manuf. 29 (2019) 100828, , https://doi.org/10.1016/j.addma.2019.100828.
[74] J.M. Arnold, C.L. Cramer, A.M. Elliott, P. Nandwana, S.S. Babu, Microstructure evolution during near-net-shape fabrication of NixAly-TiC cermets through binder jet additive manufacturing and pressureless melt infiltration, Int. J. Refract. Met. Hard Mater. 84 (2019) 104985, , https://doi.org/10.1016/j.ijrmhm.2019.104985.
[75] W. Lengauer, I. Duretek, V. Schwarz, C. Kukla, M. Kitzmantel, E. Neubauer, C. Lieberwirth, V. Morrison, Preparation and properties of extrusion-based 3D-Printed hardmetal and cermet parts, WorldPM 2018 (2018) 938–945.
[76] P. Chivavibul, M. Watanabe, S. Kuroda, K. Shinoda, Effects of carbide size and Co content on the microstructure and mechanical properties of HVOF-sprayed WC-Co coatings, Surf. Coatings Technol. 202 (2007) 509–521, https://doi.org/10.1016/j.surfcoat.2007.06.026.
[77] H.C. Lee, J. Gurland, Hardness and deformation of cemented tungsten carbide, Mater. Sci. Eng. 1 (1978) 125–133, https://doi.org/10.1016/0025-5416(78)90163-5.
[78] D. Gu, H. Wang, G. Zhang, Selective laser melting additive manufacturing of Ti-based nanocomposites: the role of nanopowder, Metall. Mater. Trans. A 45 (2014) 464–476, https://doi.org/10.1007/s11661-013-1968-4.
[79] B. AlMangour, D. Grzesiak, J.M. Yang, Selective laser melting of TiC reinforced 316L stainless steel matrix nanocomposites: influence of starting TiC particle size and volume content, Mater. Des. 104 (2016) 141–151, https://doi.org/10.1016/j.matdes.2016.05.018.
[80] C. Feng, V. Guipont, M. Jeandin, O. Amsellem, F. Pauchet, R. Saenger, S. Bucher, C. Iacob, B4C/Ni composite coatings prepared by cold spray of blended or CVD-coated powders, J. Therm. Spray Technol. 21 (2012) 561–570.
[81] W.Y. Li, C. Zhang, H. Liao, J. Li, C. Coddet, Characterizations of cold-sprayed Nickel-Alumina composite coating with relatively large Nickel-coated Alumina powder, Surf. Coatings Technol. 202 (2008) 4855–4860, https://doi.org/10.1016/j.surfcoat.2008.04.076.
[82] C.M. Fernandes, V.M. Ferreira, A.M.R. Senos, M.T. Vieira, Stainless steel coatings sputter-deposited on tungsten carbide powder particles, Surf. Coatings Technol. 176 (2003) 103–108, https://doi.org/10.1016/S0257-8972(03)00021-5.
[83] B. AlMangour, D. Grzesiak, J.M. Yang, Effect of scanning methods in the selective laser melting of 316L/TiC nanocomposites, 27th Annu. Int. Solid Free. Fabr. 2016 Proc. 26th Annu. Int. Solid Free. Fabr. Symp. – An Addit. Manuf. Conf. Rev. Pap. Eff. (2016) 566–573, https://doi.org/10.1016/j.msea.2007.05.125.
[84] S.I. Cha, S.H. Hong, B.K. Kim, The comprehensive mechanical properties of nano-

WC-Co, Mater. Sci. Eng.A 351 (2003) 31–38.
[85] S.W. Huang, M. Samandi, M. Brandt, Abrasive wear performance and microstructure of laser clad WC/Ni layers, Wear. 256 (2004) 1095–1105, https://doi.org/10.1016/S0043-1648(03)00526-X.
[86] S. Das, T.P. Fuesting, G. Danyo, L.E. Brown, J.J. Beaman, D.L. Bourell, Direct laser fabrication of superalloy cermet abrasive turbine blade tips, Mater. Des. 21 (2000) 63–73, https://doi.org/10.1016/s0261-3069(99)00057-6.
[87] J.M. Castanho, M.T. Vieira, C.M. Fernandes, A.M.R. Senos, M. Matos, Coated WC powders by sputtered nanostructured Ni and stainless steel, Vacuum. 82 (2008) 1404–1406, https://doi.org/10.1016/j.vacuum.2008.03.040.
[88] H. Kim, W. Cong, H.C. Zhang, Z. Liu, Laser engineered net shaping of nickel-based superalloy inconel 718 powders onto aisi 4140 alloy steel substrates: interface bond and fracture failure mechanism, Materials (Basel). 10 (2017) 341–358, https://doi.org/10.3390/ma10040341.
[89] B.D. Kernan, E.M. Sachs, M.A. Oliveira, M.J. Cima, Three-dimensional printing of tungsten carbide-10 wt% cobalt using a cobalt oxide precursor, Int. J. Refract. Met. Hard Mater. 25 (2007) 82–94, https://doi.org/10.1016/j.ijrmhm.2006.02.002.
[90] I. Konyashin, B. Ries, D. Hlawatschek, Y. Zhuk, A. Mazilkin, B. Straumal, F. Dorn, D. Park, Wear-resistance and hardness: Are they directly related for nanostructured hard materials, Int. J. Refract. Met. Hard Mater. 49 (2015) 203–211, https://doi.org/10.1016/j.ijrmhm.2014.06.017.
[91] X. Ren, H. Shao, T. Lin, H. Zheng, 3D gel-printing-An additive manufacturing method for producing complex shape parts, Mater. Des. 101 (2016) 80–87, https://doi.org/10.1016/j.matdes.2016.03.152.